Journal of Orissa Mathematical Society ISSN: 0975-2323
Vol. 37, No. 01-02, 2018, 55-76

Impact of stress jump on two phase peristaltic transport - A physiological aspect

S Shaw *and P. Sibanda †

Abstract

In this investigation we considered to extend the work of Misra and Pandey [1] by taking the permeability nature of the peripheral region and introduce a stress-jump condition at the interface of core and peripheral region present a mathematical model for the peristaltic transport in small vessels. The blood is treated as a two-phase fluid with a core region that is described by the Casson model and a porous peripheral layer that is described by the Brinkman extended Darcy model. The study shows, that a high blood flow rate introduces a trapping region in the peripheral layer while reflux occurs in the core region for increasing porosity and stress-jump constant, and a better pumping performance is obtained by reducing the Darcy number. The trapped region area increased with the stress-jump constant and the effective viscosity. However the reverse phenomena was observed for the Darcy number and porosity. The effective viscosity increases size of the trapping region. Moreover, it was observed that the Darcy number and the stress jump constant strongly affect the velocity profile more than the porosity and the yield stress. The pumping performance decreased with increases in Darcy number.

*Department of Mathematics and Statistical Sciences, Botswana International University of Science and Technology, Private Mail 16, Palapye, Botswana, email : sachinshaw@gmail.com; shaws@biust.ac.bw
†School of Mathematics, Statistics and Computer Sciences, University of KwaZulu-Natal Pietermaritzburg, KwaZulu-Natal, 3209, South Africa, email : SibandaP@ukzn.ac.za

1991 Mathematics Subject Classification: 35J25, 35K05, 76Mxx, 76Zxx.

Keywords: Casson fluid, two-phase flow, stress-jump condition, peristaltic pumping reflux, trapping region..

1 Introduction

Peristaltic transport involves the propogation of progressive wave of area contraction or expansion along the wall of a fluid-filled distensible tube. In the human body, peristaltic action is an inherent neuro-muscular property of any tubular smooth muscle structure (Jaffrin and Shapiro [2]). This mechanism is responsible for the transport of biological fluids in several physiological processes such as the passage of urine from the kidneys to the bladder, the transport of food bolus through the gastrointestinal tract (Tripathi and Beg [3]), the transport of blood in small blood vessels Misra and Pandey [4]), embryo transport in the uterus, and the movement of spermatozoa in the reproductive tract (Batra [5]). It has been suggested that impaired peristalsis may result in the transport of bacteria (Pozrikidis [6]) and infertility (Macht [7]). Peristaltic transport is also useful in the design of pumps used in the transportation of corrosive or dangerous fluids and biomedical systems. Many modern medical devices are designed on the principle of peristaltic pumping to transport fluids without internal moving parts, for example, the blood in the heart-lung machine. In the present problem we mainly focus on the vasomotion flow that is prevalent in the entire microcirculatory system.

Chakravarty and Mandal [8] studied a two dimensional blood flow through a tapered stenosed artery by considering blood as Newtonian fluid. Peristaltic flow Later Mandal [9] extended the work for non-Newtonian power-law fluid for unsteady flow. Shaw et al. [10] studied a two dimensional blood flow through a stenosed artery by considering blood as Casson fluid. Deshikachar and Rao [11] studied the effect of the magnetic field on the flow and blood oxygenation in the channel of variable cross section. They are considered the pulsatile flow of blood with channel wall as a function of axial coordinate. Mekheimer [12] studied the peristaltic flow of blood in a non-uniform channels in presence of magnetic

field. He considered non-Newtonian Couple-Stress fluid as blood. Many Researchers are investigated the peristaltic blood flow through the small artery using a two phase fluid model for blood and they observed that the peripheral layer highly influenced the peristaltic blood flow (Usha and Rao [13]). Permeability plays a vital role in the peristaltic transport phenomena (Akbar et al. [14]). Bhatti et al. [15] have studied the impact of slip effect on the blood flow induced by peristaltic wave and presented as endoscopy analysis on the system. Bhatti et al. [16] shows the influence of the permeability and interface conditions for a two phase peristaltic flow in a porous medium. Peristaltic flow is very significant in the channel flow mainly when deals with porous medium (Mohammadein and Abu-Nab [17]).

Precious most of the problem based on the single phase peristaltic flow of Newtonian or non-Newtonian fluid. The present problem deals with a two phase flow. Mishra and Pandey [1] investigated the peristaltic blood flow through the small artery using a two phase fluid model by considering Casson fluid at the core region and Newtonian fluid at the peripheral layer which is impermeable in nature. The objective of the present paper is to investigate the significance of permeability of microvessel, stress jump condition on peristaltic transport of blood. The trapping and pumping characteristics are discussed for different parameters in the model which will give a clear view on the blood transport in microvessel.

2 Mathematical Formulation

We Consider a two dimensional peristaltic transport in a channel surrounded by a glycocalyx based peripheral layer. The walls of the channel are assumed to be flexible and peristaltic propagating wave is represented by a sinusoidal wave in fixed frame with amplitude b, wavelength λ and a constant speed c in the axial direction and written as

$$Y = \pm H(X - ct) = \pm \left[d + b \sin \frac{2\pi}{\lambda}(X - ct) \right],$$

where $2d$ is the mean channel width. The interface of the plug and the core region, and the core and peripheral regions are denoted by $Y = \pm H_p(X - ct)$ and $Y = \pm H_1(X - ct)$, respectively as shown in Fig.

1.

At the core, the blood behaves as a non-Newtonian Casson fluid with density ρ_1 and viscosity μ_1, and in the peripheral layer it behaves as an incompressible Newtonian fluid with density ρ_2 and viscosity μ_2. Due to glycocalyx, the peripheral layer is highly negatively charged and this is included as a body force term in the momentum equation. We assume the peripheral layer is isotropic and homogeneous. The boundary shape does not remain constant in the unsteady laboratory frame. We further assume that that the pressure difference across the ends of the channel is unaltered and the period of the interfaces and peristaltic wave are same. Using a transformations from the fixed frame such a way that the flow becomes steady in a wave frame of reference (x,y) moving with speed c in the direction of the wave propagation, written as

$$x = X - ct,\ y = Y,\ u_i = U_i - c,\ v_i = V_i,\ p_i(x) = P_i(X,t), \tag{2.1}$$

where (u_i, v_i) and (U_i, V_i) are defined the velocity component in the axial and transverse directions, in the wave and fixed frames of reference.The subscript i takes the value 1 for the core layer and 2 for the glycocalyx based peripheral layer. The equations of the Casson fluid suggested by Casson [18] are

$$\sqrt{\tau} = \sqrt{\mu_c \dot{\gamma}} + \sqrt{\tau_y} \qquad \tau \geq \tau_y, \dot{\gamma} = 0, \qquad \tau \leq \tau_y, \tag{2.2}$$

where τ is the shear stress, $\dot{\gamma}$ is the strain rate, τ_y is the yield stress and μ_c is the Casson viscosity.

2.1 Effective Viscosity

When blood flow through the microvessel, the apparent viscosity of the blood simultaneously depends on the hematocrit and diameter of the microvessel mainly when the diameter of the microvessel smaller than $40\mu m$ (Fahraeus [19]; Fahraeus and Lindqvist [20]). This happen due to the axial accumulation of the RBCs which form a lower viscosity plasma skimming cell-depleted region near the microvessel wall. We use the experimentally determined analytic formula given by Pries et al. [21] for effective blood

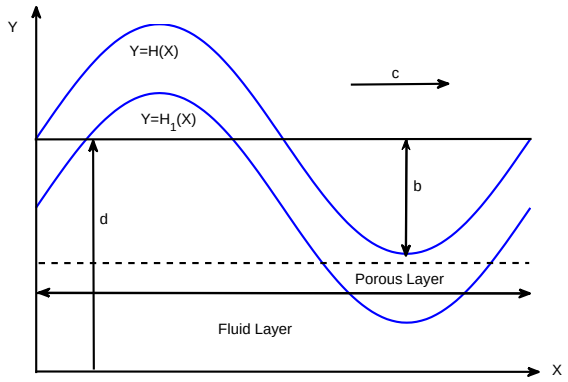

Figure 1: Peristaltic motion at the microvessel wall

viscosity as

$$\mu_1 = \mu_2 \left[1 + (\mu_{0.45} - 1) \frac{(1-H_D)^C - 1}{(1-0.45)^C - 1} \right) \left(\frac{d_v}{d_v - 1.1} \right)^2 \Bigg] \times \left(\frac{d_v}{d_v - 1.1} \right)^2, \tag{2.3}$$

where μ_2 is the viscosity of the blood plasma or the peripheral layer, d_v is the diameter of the microvessel in micrometer (μm), H_D is the hematocrit of blood, d_v is the diameter of the vessel and the other constants are $\mu_{0.45} = 6e^{-0.085 d_v} + 3.2 - 2.44 e^{-0.06 d_v^{0.645}}$ and $C = \left(0.8 + e^{-0.075 d_v}\right) \left(\frac{1}{1+10^{-11} d_v^{12}} - 1 \right) + \frac{1}{1+10^{-11} d_v^{12}}$

2.2 Fluid flow equation

When the wavelength is large, the Reynolds number $Re = d^2 c \rho_1 / \lambda \mu_1$ is quite small, and therefore the initial convection acceleration terms may be neglected in comparison with viscous terms. We are using the following set of non-dimensional quantities

$$\bar{x} = x/\lambda,\ \bar{y} = y/d,\ \bar{t} = ct/\lambda,\ \bar{p}_i = d^2 p_i / \mu_1 c\lambda,\ \bar{u}_i = u_i/c,\ \bar{v}_i = v_i / c\delta,\ \delta = d/\lambda,$$

$$h = H/d,\ h_p = H_p/d,\ h_1 = H_1/d,\ \mu = \mu_2/\mu_1,\ \rho = \rho_1/\rho_2,\ \bar{\Psi}_i = \Psi_i/dc,\ \bar{\tau}_y = d\tau_y/c\mu_1,$$

$$\bar{\kappa} = d\kappa. \tag{2.4}$$

Using the above assumption and non-dimensional quantities, the non-dimensional governing equa-

tion of motion in the fluid core region ($0 \le y \le h_1$) is written (dropping the bar for convenience) as

$$\frac{\partial u_1}{\partial x} + \frac{\partial v_1}{\partial y} = 0, \tag{2.5}$$

$$\frac{\partial u_1}{\partial y} = 0, \quad 0 \le y \le h_p, \tag{2.6}$$

$$\frac{\partial p_1}{\partial x} = -\frac{\partial}{\partial y}\left[-\frac{\partial u_1}{\partial y} + \tau_y + 2\sqrt{-\tau_y \frac{\partial u_1}{\partial y}}\right], \quad h_p \le y \le h_1. \tag{2.7}$$

Using the Darcy-Brinkman model for the peripheral layer including the electrokinetic force as a body force, the non-dimensional governing equation at the porous region ($h_1 \le y \le h$)is written (dropping the bar for convenience) as

$$\frac{\partial u_2}{\partial x} + \frac{\partial v_2}{\partial y} = 0, \tag{2.8}$$

$$\frac{\partial p_2}{\partial x} = \frac{\mu}{\varepsilon}\frac{\partial^2 u_2}{\partial y^2} - \frac{\mu}{K}u_2, \tag{2.9}$$

where ε and K are the porosity and permeability in the porous region, respectively. We introduce the stream function Ψ_i where $u_i = \partial\Psi_i/\partial y$ and $v_i = -\partial\Psi_i/\partial x$, and eliminating the pressure gradient we get

$$\Psi_{1yy} = 0, \quad 0 \le y \le h_p, \tag{2.10}$$

$$\left[-\Psi_{1yy} + \tau_y + 2\sqrt{-\tau_y \Psi_{1yy}}\right]_{yy} = 0, \quad h_p \le y \le h_1, \tag{2.11}$$

$$\Psi_{2yyyy} - \alpha^2 \Psi_{2yy} = 0, \quad h_1 \le y \le h, \tag{2.12}$$

where $\alpha^2 = \varepsilon/Da$, $Da = K/d^2$ is the Darcy number. The subscript y represent the partial derivative with respect to that term. By considering the no-slip condition at the wall, conservation of mass at the peripheral layer, maximum and constant velocity at the center of the axis, the non-dimensional boundary conditions at the wall and axis of the microvessel are written as

$$\Psi_{2y} = -1, \ \Psi_2 = q, \quad \text{at } y = h(x), \tag{2.13}$$

$$\Psi_{1yy} = 0, \ \Psi_1 = 0 \quad \text{at } y = 0. \tag{2.14}$$

At the interface of the clear fluid region and porous region i.e., at $y = h_1(x)$, we are considered the conservation of mass, continuity of the velocity, stress-jump condition and continuity of pressure gradient which can written in the non-dimensional form as

$$\Psi_1 = \Psi_2 = q_1, \text{ (conservation of mass)} \tag{2.15}$$

$$\Psi_{1y} = \Psi_{2y}, \text{ (continuity of velocity)} \tag{2.16}$$

$$\Psi_{1yy} = \mu_\varepsilon \left(\Psi_{2yy} - \beta_1 \Psi_{2y}\right), \text{ (stress-jump condition)}, \tag{2.17}$$

$$\Psi_{1yyy}\left(1 + \sqrt{-\tau_y/\Psi_{1yy}}\right) = \mu_\varepsilon(\Psi_{2yyy}, \text{(normal stress)} \tag{2.18}$$

where q and q_1 in (2.13) and (2.15) are the total and core fluxes, respectively, $\mu_\varepsilon = \mu/\varepsilon$ and $\beta_1 = \beta\varepsilon/\sqrt{Da}$.

2.3 Solution of the problem

We obtain the stream function at the core and the peripheral region by solving the equations (2.11) and (2.12) using the corresponding boundary conditions (2.13)-(2.18) as

$$\Psi_1(x,y) = -\frac{A(x)y^3}{6} - \tau_y y^2 - \frac{8\sqrt{\tau_y}}{15(A(x))^2}\left[(A(x)y + \tau_y)^{5/2} - {\tau_y}^{5/2}\right] + Cy, \tag{2.19}$$

$$\begin{aligned}\Psi_2(x,y) = q - (y-h) + N_1\left[\sinh(\kappa y) - \sinh(\kappa h) - \kappa(y-h)\cosh(\kappa h)\right] \\ + G\left[\cosh(\alpha y) - \cosh(\alpha h) - \alpha(y-h)\cosh(\alpha h)\right] \\ + H\left[\sinh(\alpha y) - \sinh(\alpha h) - \alpha(y-h)\cosh(\alpha h)\right],\end{aligned} \tag{2.20}$$

where the constants C, G, H and $N_i (i = 1, 2, ..., 8)$ are given in the Appendix. The stream function at the plug region $(0 \le y \le h_p)$ is determined as

$$\Psi_p(x,y) = \left[-\frac{A(x){h_p}^2}{6} - \tau_y h_p - \frac{8\sqrt{\tau_y}}{15(A(x))^2 h_p}\left((A(x)h_p + \tau_y)^{5/2} - {\tau_y}^{5/2}\right) + C\right] y, \tag{2.21}$$

We can determine the value of $A(x)$ from the following equation

$$0 = k_1 (A(x))^3 + k_2 (A(x))^2 + \sqrt{\tau_y} (A(x))^3 (A(x)h + \tau_y)^{-1/2} + \sqrt{\tau_y}(A(x))^3 \left[A(x)h_1 + 2\tau_y + 2\sqrt{\tau_y(A(x)h_1 + \tau_y)}\right]^{-1/2} (1 + \sqrt{\tau_y} (A(x)h_1 + \tau_y)^{-1/2}) + k_3(A(x))^2 (A(x)h_1 + \tau_y)^{1/2} + k_4 (A(x)h_1 + \tau_y)^{5/2} + k_5(A(x)) (A(x)h_1 + \tau_y)^{3/2} + k_6, \quad (2.22)$$

where the constants k_i $(i = 1, \ldots, 6)$ are given in the Appendix. Using the secant method we can easily solve this equation to find the appropriate value of $A(x)$. The non-dimensional flux Q at any axial direction as function of the flux q in the wave form is defined as

$$Q = \int_0^h (u+1)dy = q + h. \quad (2.23)$$

The average volumetric flow rate of the peristaltic wave over one period ($T = \lambda/c$)is obtained as

$$\bar{Q} = \frac{1}{T}\int_0^T Q dt = \frac{1}{T}\int_0^T (q + h(x,t))dt = q + \int_0^1 h dx. \quad (2.24)$$

The interface between the porous and fluid region is a streamline which should satisfied the conservation of mass in both region as mention in condition (2.15) and it is not known *apriori*. Using equation (2.15) and solving any one of the stream functions Ψ_1 or Ψ_2. For simplicity, using $\Psi_2 = q_1$ which give the equation for the interface $h_1(x)$ as

$$k(h_1) = q_1 - q + N_1(\sinh(\kappa h) - \sinh(\kappa h_1)) - (h - h_1)(1 + N_1 \kappa \cosh(\kappa h)) + G[\cosh(\alpha h) - \cosh(\alpha h_1) - (h - h_1)\alpha \sinh(\alpha h)] + H[\sinh(\alpha h) - \sinh(\alpha h_1) - (h - h_1)\alpha \cosh(\alpha h)] = 0, \quad (2.25)$$

where q and q_1 are constants i.e., independent of x. Using $h_1 = \gamma$ at $x = 0$ in (2.25) we get

$$q_1 = \frac{(1-\gamma)M_9 + (\bar{Q} - 1)M_6 + M_3[M_{10}(M_2M_3 - M_1M_4) + M_{11}(M_{12} + M_{13})] - M_1M_5M_{14}}{M_3(M_1M_4 - M_2M_3)}, \quad (2.26)$$

where the constants $M_i (i = 1, \ldots, 14)$ are given in the Appendix. Equation (2.25) is a transcendental equation and may have many positive real roots. The interface of the porous and fluid region is well defined if it contain a single root in the interval $0 \leq h_1 \leq h$ and satisfied the equation (2.24). From the equation (2.25), we obtained the boundary values $k(h_1)$ as $k(0) = q_1$ and $k(h) = -q_2 = q_1 - q$. Depending on the sign of q_1 and q_2, three different cases may arise (i) if both $q_1, q_2 > 0$ or < 0, then there exist at least one non-zero real root or an odd number of roots. A single root in the given interval assured an unique interface which is independent γ, (ii) if q_1 and q_2 are of opposite sign then there exist an even number or no real roots in the domain. So the interface is not unique, and (iii) if either q_1 or q_2 is zero, then there exist a non-zero even or odd number of real roots which depends on the function $k(h_1)$ as it is decreasing or increasing function near $y = 0$ and $y = h$ (Mishra and Rao [22]).

3 Results and discussions

In this study we used both analytical and numerical methods to solve the governing equations. To find the root of the equations we used the secant method and integrated using Simpson's 1/3 rule. We used the following parameter values; the blood yield stress is $0.0004 N/m^2$, the peripheral layer thickness (average) is $1.5 \mu m$, the Casson viscosity for the core region $\mu_1 = 3.5$cp, the viscosity at the peripheral layer $\mu_2 = 1.02$cp at 39% hematocrit and the radius of the microvessel is $5 \mu m$.

3.1 Trapping

For certain combinations of the phase angle ϕ and $\bar{Q}$ there is a region of closed streamlines. This region experiences a recirculation and moves with a mean speed equal to that of the wave. This is termed the trapping region. Peristalsis exhibits this phenomenon when the tube is sufficiently occluded. We set $\Psi_1 = 0$ for $y > 0$ in equation (2.19) to determine the trapping range. This gives the polynomial of order

five;

$$25A^6y^5 - A^3\tau_y(64A^2+150)y^4 + A^4(-95{\tau_y}^2+150AC)y^3 - A^3\tau_y(560{\tau_y}^2+450AC)y^3 + A^2(225A^2C^2-880{\tau_y}^4) + A{\tau_y}^4(240AC-320{\tau_y}^2) = 0, \quad (3.27)$$

for an appropriately chosen $0 < y < h$. The presence of center streamline trapping is associated with the existence of stagnation points in the wave frame at the center line where the velocity components u_1 and v_1 both disappeared. The stagnation points are calculated from (2.19) using the following conditions given as

$$u_1|_{y=0} = v_1|_{y=0} = 0, \quad (3.28)$$

which implying that

$$\bar{Q} = \frac{(1+h+N_{15})N_6N_{16} - N_{16}(N_5N_6 - N_2N_8) - N_{12}(N_{17}N_6 - N_8N_{18})}{N_6N_{16}}. \quad (3.29)$$

We calculating the upper trapping limit $\bar{Q}_u$ and the lower trapping limit $\bar{Q}_l$ by substituting h and h_1 at $x = 0.25$ and $x = 0.75$ in the above equation, respectively and get center line trapping lying between $\bar{Q}_l$ and $\bar{Q}_u$. Equations (3.25) and (3.29) were solved simultaneously and the values of the lower and upper trapping limits found.

The lower trapping limit function of the phase angle for different value of Darcy number Da, porosity ε, shear-stress jump constant β and viscosity ratio μ is shown in Figs. 2(a)-2(d). It is evident that the lower trapping limit is a non-linear function of the phase angle. The trapped region area increases with the shear stress jump constant β and the viscosity μ. However, the reverse is observed for the Darcy number Da and the porosity ε. The lower trapping limit initially increases up to a certain point and then decreases with the phase angle.

The effect of the Darcy number on the streamlines in the wave frame is shown in Fig. 3 when $\bar{Q} = 0.6, \mu = 0.343, \phi = 0.6, \gamma = 0.7, \beta = 0.5$ and $\varepsilon = 0.7$. Here the trapping region decreases as the Darcy number decreases and when $Da \leq 0.1$ no trapped region develops. Increasing the viscosity ratio

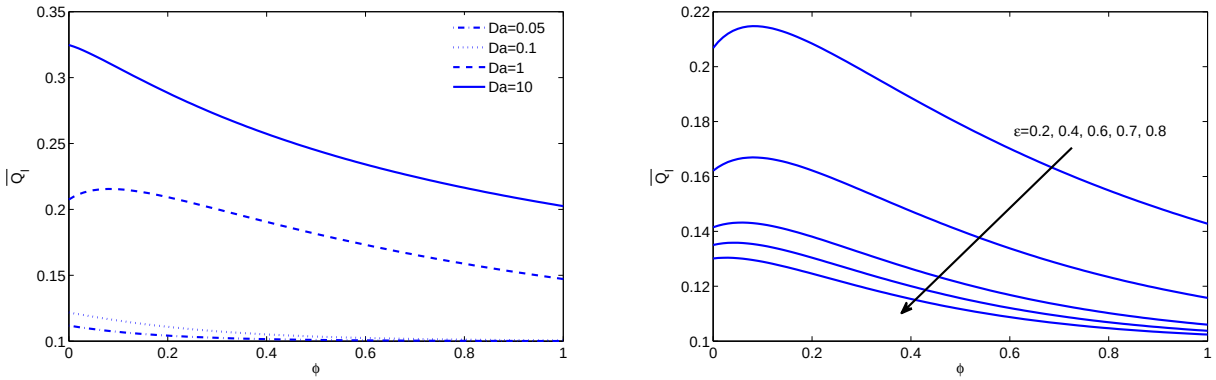

Figure 2: The lower trapping limit vs. the phase angle when $\gamma = 0.7, \tau_y = 0.001$ (a) for different Da ($\varepsilon = 0.3, \mu = 0.343, \beta = 0.1$) (b) for different ε ($\beta = 0.1, \mu = 0.343, Da = 0.5$).

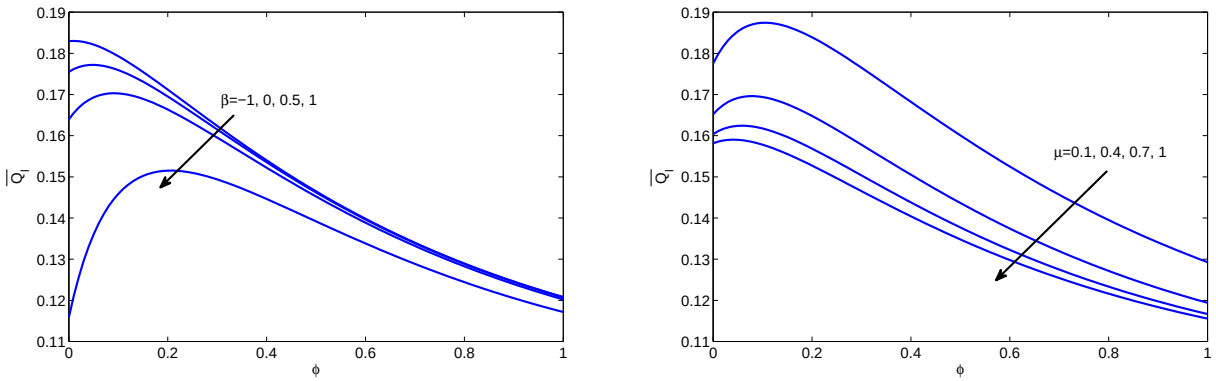

Figure 3: The lower trapping limit vs. the phase angle when $\gamma = 0.7, \tau_y = 0.001$ (a) for different β ($\varepsilon = 0.3, \mu = 0.343, Da = 0.5$) (b) for different μ ($\beta = 0.1, \varepsilon = 0.3, Da = 0.5$).

μ increases the size of the trapping region, a similar phenomena observed for bolus transport in the gastrointestinal tract as reported by Rao and Mishra [22].

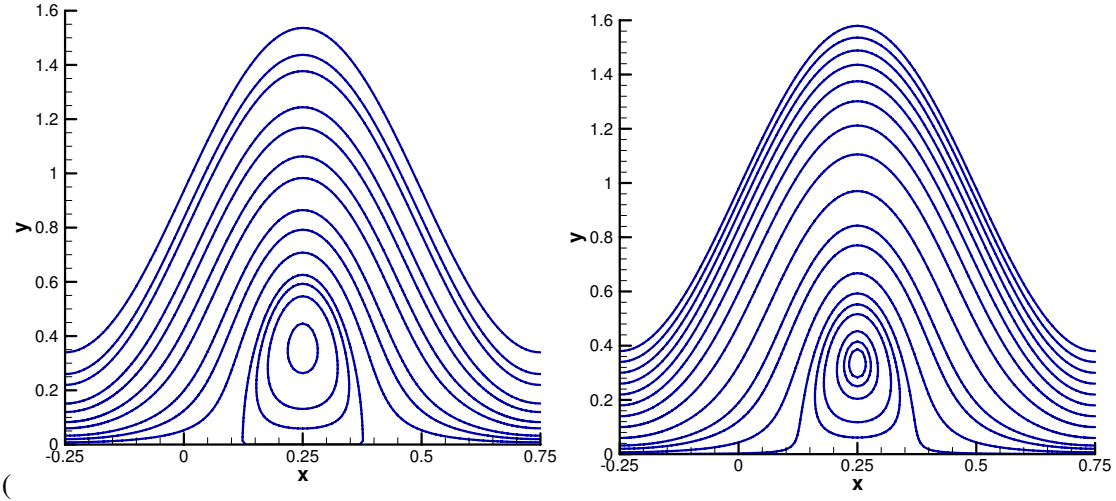

(

Figure 4: Streamlines in the wave frame with $\bar{Q} = 0.6, \mu = 0.343, \phi = 0.6, \varepsilon = 0.7, \gamma = 0.7, \beta = 0.5$ (a) $Da = 10$ (b) $Da = 4$.

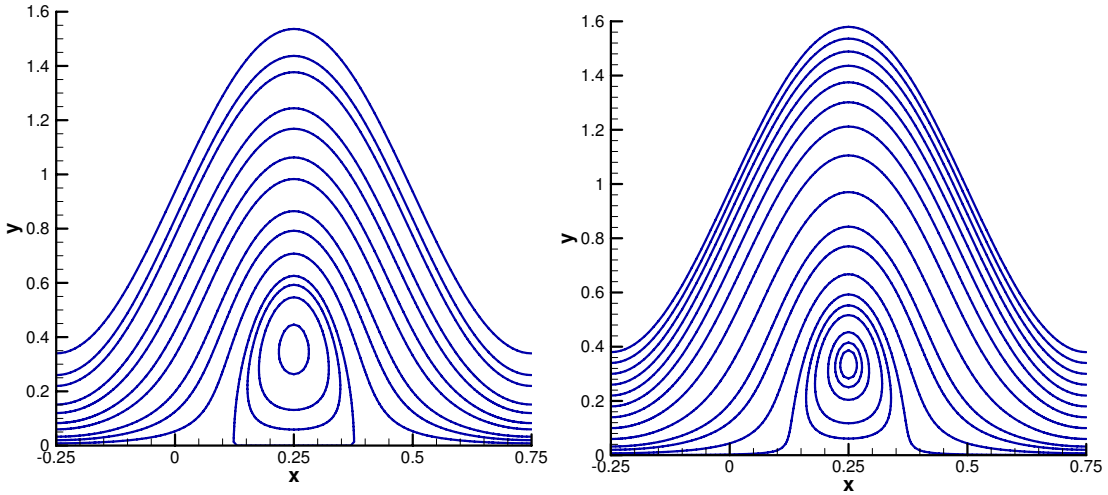

Figure 5: Streamlines in the wave frame with $\bar{Q} = 0.6, \mu = 0.343, \phi = 0.6, \varepsilon = 0.7, \gamma = 0.7, \beta = 0.5$ (a) $Da = 10$ (b) $Da = 4$.

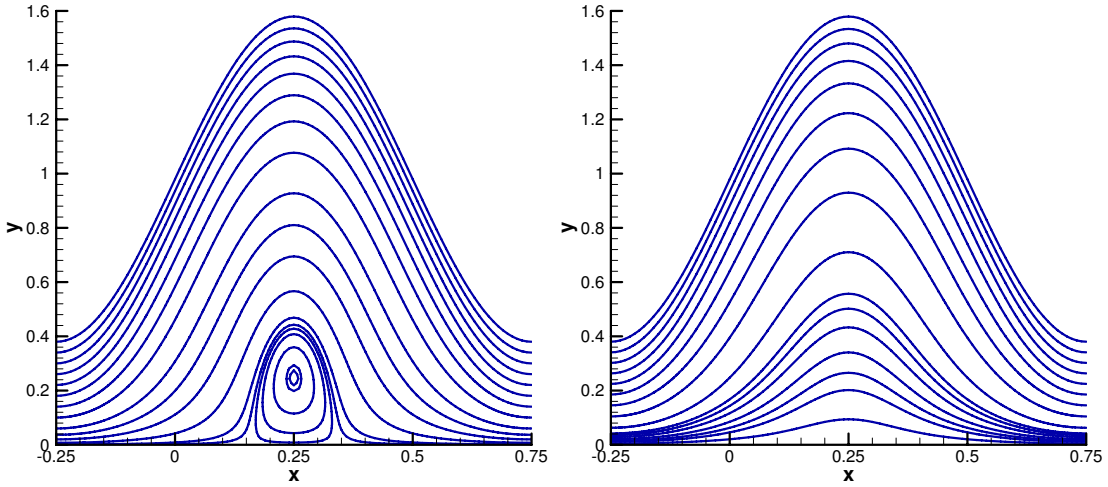

Figure 6: Streamlines in the wave frame with $\bar{Q} = 0.6, \mu = 0.343, \phi = 0.6, \varepsilon = 0.7, \gamma = 0.7, \beta = 0.5$ (a) $Da = 1$ (b) $Da = 0.1$.

3.2 Reflux and axial velocity

Reflux is a phenomena which refers to the presence of fluid particles whose mean motion over one cycle is against the net pumping direction. This phenomenon is of physiological importance as it may imply a possible backward motion of bacteria against the direction of the physiological fluids. We define a non-dimensional volume flow rate Q_Ψ which define the material particles in a fixed frame. Between the axis of the channel and the wave frame streamline Ψ, the volume flow rate is written as

$$Q_\Psi = \Psi + y(\Psi, x, t). \tag{3.30}$$

Averaging Q_Ψ over one period of the wave, we obtain

$$\bar{Q_\Psi} = \Psi + \int_0^1 y(\Psi, x)dx. \tag{3.31}$$

Normalized the average Q_Ψ and stream function using the following definitions as $Q^* = \bar{Q_\Psi}/\bar{Q_w}$, $\Psi^* = \Psi/\Psi_w$, where $\bar{Q_w}$ and Ψ_w are represent the flow rate and the stream function at the vessel wall (i.e., $y = h(x,t)$) where $\bar{Q_w} = \bar{Q}$ and $\Psi_w = \bar{Q} - 1 = q$. If Q^* is an increasing function of Ψ^* then the particle motion always towards the pumping direction. However if Q^* is a decreasing function of Ψ^* then reflux appears

in that region. With a given constant value Ψ, we solve the equations (2.19) and (2.20) numerically by considering y as a function of x.

The reflux phenomena in Q^* as a function of Ψ^* is shown in Fig. 5 for different values of the Darcy number, stress jump constant, porosity and yield stress. In all cases Q^* varies nonlinearly with Ψ^*. It is observed that the reflux appears for small Darcy numbers and Ψ^*. Otherwise Q^* is a strictly increasing function of the Darcy number. The reflux however appeared for higher values of the stress-jump constant β. It is evident that Q^* is a strictly increasing function of Ψ^* when $\beta = 0$. Q^* decreases for lower values of Ψ^* but then increases non-linearly with Ψ^* for non-zero β. The same phenomena is shown for the porosity parameter ε. The effect of the yield stress on Q^* is shown in Fig. 5(d) for $Da = 0.01$. The value of Q^* is less when considering the non-Newtonian fluid at the core region than for the Newtonian case.

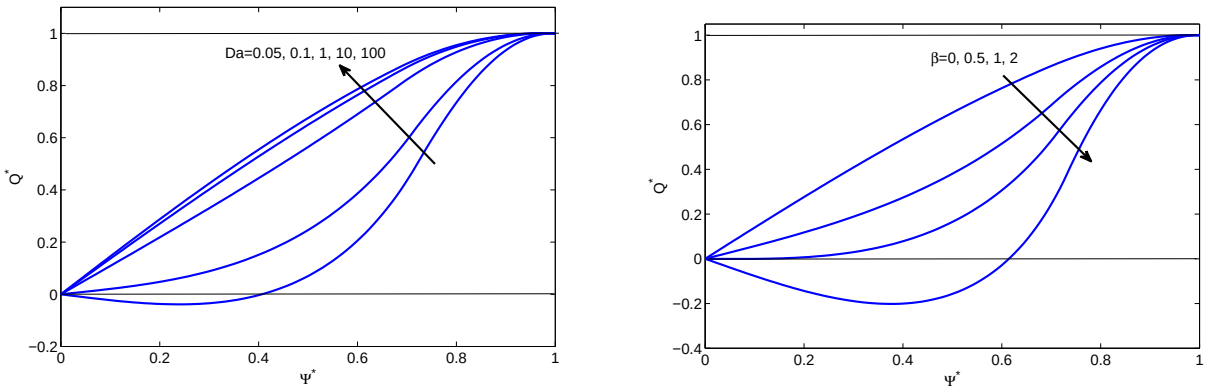

Figure 7: The reflux phenomenon Q^* vs. Ψ^* with $\mu = 0.343, \phi = 0.6, \bar{Q} = 0.1, \gamma = 0.7$ (a) for different Da ($\varepsilon = 0.3, \beta = 0.1, \tau_y = 0.001$) (b) for different β ($\varepsilon = 0.8, Da = 0.5, \tau_y = 0.001$).

The axial velocity u of the fluid is calculated by differentiating Eqs. (2.19) and (2.20) with respect to y for the core region (u_1)and the peripheral region (u_2), respectively. This is given by

$$u_1 = \frac{A(x)y^2}{2} - 2\tau_y y - \frac{4\sqrt{\tau_y}}{3A(x)}(A(x)y + \tau_y)^{3/2} + C, \tag{3.32}$$

$$u_2 = -1 + N_1\kappa\left[\cosh(\alpha y) - \cosh(\alpha h)\right] + G\alpha\left[\sinh(\alpha y) - \cosh(\alpha h)\right] + H\alpha\left[\cosh(\alpha y) - \cosh(\alpha h)\right]. \tag{3.33}$$

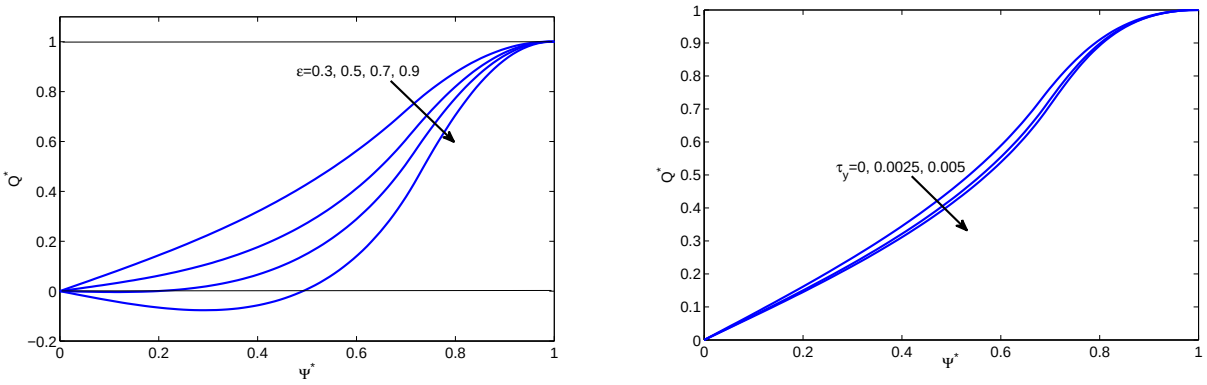

Figure 8: The reflux phenomenon Q^* vs. Ψ^* with $\mu = 0.343, \phi = 0.6, \bar{Q} = 0.1, \gamma = 0.7$ (a) for different ε ($\beta = 0.8, Da = 0.05, \tau_y = 0.001$) (b) for different τ_y ($\phi = 0.5, \beta = 0.7, \varepsilon = 0.8, Da = 0.01$).

The axial velocity is plotted in Fig. 6 for different Darcy numbers, porosity, stress-jump constant and yield stress. It is observed that the Darcy number and the stress-jump constant more strongly influence the velocity profile than does the porosity and the yield stress. The kinks in the graphs show points on the interface where the shear stress is discontinuous. A flow reversal appears in the core region for $Da = 0.01, \beta = 0, 0.5$ and all values of τ_y indicating a possible reflux in that region as observed in Fig. **??**. Near $y = 0$, the velocity profiles are parallel to the y-axis an indication of the yield stress.

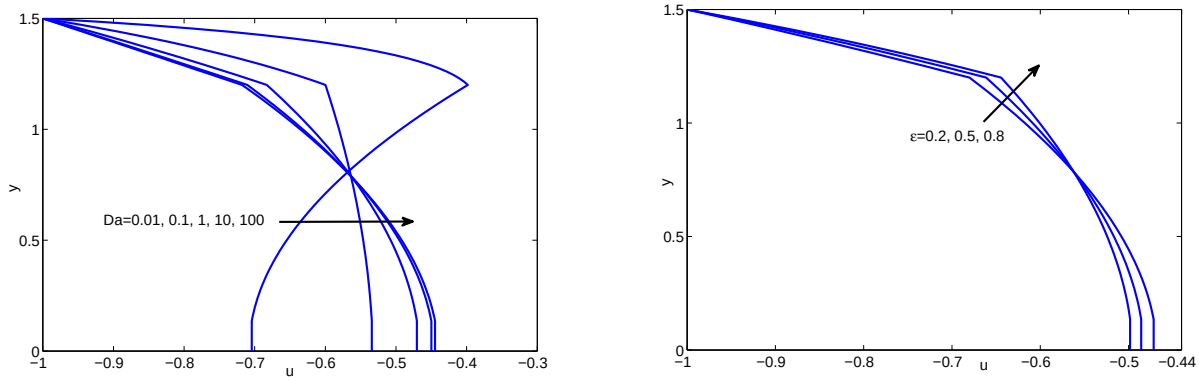

Figure 9: Axial velocity at $x = 0.25$ with $\phi = 0.5, \gamma = 0.7, \bar{Q} = 0.5, \mu = 0.343$ (a) for different Da ($\varepsilon = 0.7, \beta = 0.5, \tau_y = 0.001$) (b) for different ε ($\beta = 0.5, \tau_y = 0.001, Da = 0.5$).

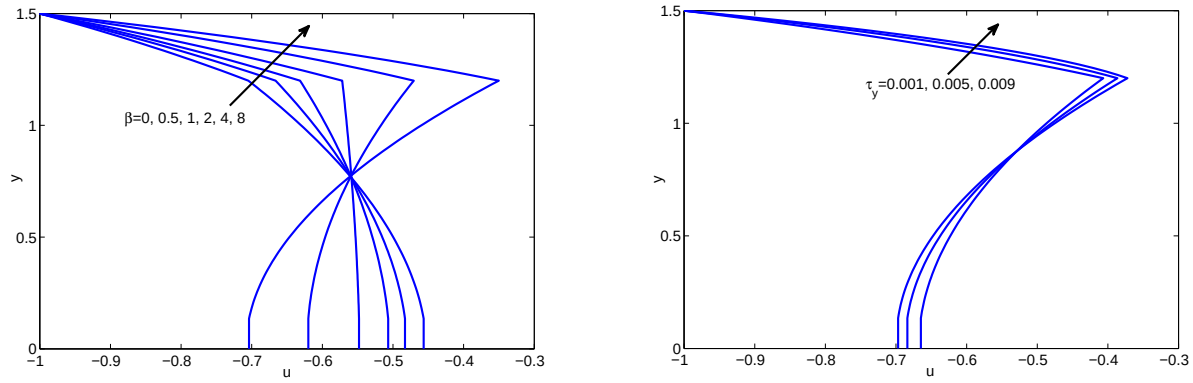

Figure 10: Axial velocity at $x = 0.25$ with $\phi = 0.5, \gamma = 0.7, \bar{Q} = 0.5, \mu = 0.343$ (a) for different β ($\varepsilon = 0.7, \tau_y = 0.001, Da = 0.5$) (b) for different τ_y ($\beta = 5, \varepsilon = 0.9, Da = 0.5$).

3.3 Pumping characteristics

Substituting (2.19) and (2.20) in the momentum equation, we get the pressure gradients at the core and the peripheral region as

$$\frac{\partial p_1}{\partial x} = A + A\sqrt{\tau_y}(Ay+\tau_y)^{-1/2} + A(\tau_y+\sqrt{\tau_y})(Ay+2\tau_y+2\sqrt{Ay\tau_y+\tau_y{}^2}), \tag{3.34}$$

$$\frac{\partial p_2}{\partial x} = \mu_\varepsilon \kappa N_1(\kappa^2-\alpha^2)\cosh(\kappa y) + \frac{\mu}{Da}(1+N_1\kappa\cosh(\kappa h)) + \frac{\mu\alpha}{Da}(G+H)\cosh(\alpha h) + F_e. \tag{3.35}$$

The pressure difference for one wavelength is found by integrating equations (3.34) and (3.35)

$$\Delta P = p_1 - p_0 = \int_0^1 (A + A\sqrt{\tau_y}(Ay+\tau_y)^{-1/2} + A(\tau_y+\sqrt{\tau_y})(Ay+2\tau_y+2\sqrt{Ay\tau_y+\tau_y{}^2}))dx. \tag{3.36}$$

Using numerical quadrature formulae from equation (3.36),we calculate average flow rate $\bar{Q}$ as a function of Δp. The maximum pressure difference Δp_0, obtained by putting $\bar{Q} = 0$ in above equation. The effect of various parameters such as the Darcy number, porosity, stress-jump constant and viscosity ratio on the pumping characteristics is shown in Fig. 7. It is observed that at the pumping region, the pumping efficiency increases ($\Delta p > 0$) with decrease in Darcy number.It is interesting to note that the pumping efficiency is less for the clear fluid as the porous region becomes a clear fluid region for large value of Darcy number i.e., the permeability of the peripheral region is tending to infinity. It is observed that Δp

is a linear function of Q. The effect of the porosity on the pumping characteristics is shown in Fig. 7(b). The pumping characteristics is a decreasing function of porosity ε but it increases for larger values of a critical Δp and a flow reversal occurs for a smaller value of the critical Δp. Similar results are obtained at the co-pumping region ($\Delta p < 0$). All the curves intersect at a critical point. The position of this critical point depends on the value of the other parameters. In the present study, we have considered Brinkmann extended Darcy model in the peripheral region where the porosity lies between 0 and 1, (Nield [23]). It is also evident that for large values of the porosity, shows a bigger flux in free pumping and copumping. The average volumetric flow rate $\bar{Q}$ increases with an increase in the value of stress jump constant β for a fixed Δp. However a reversal phenomena evident at lower values of Δp which clearly depicted from Fig. 7(c). With an increase in the viscosity, the critical Δp increases as shown in Fig. 7(d). An interesting observation here is that all the curves intersect at the free pumping ($\Delta p = 0$) region.

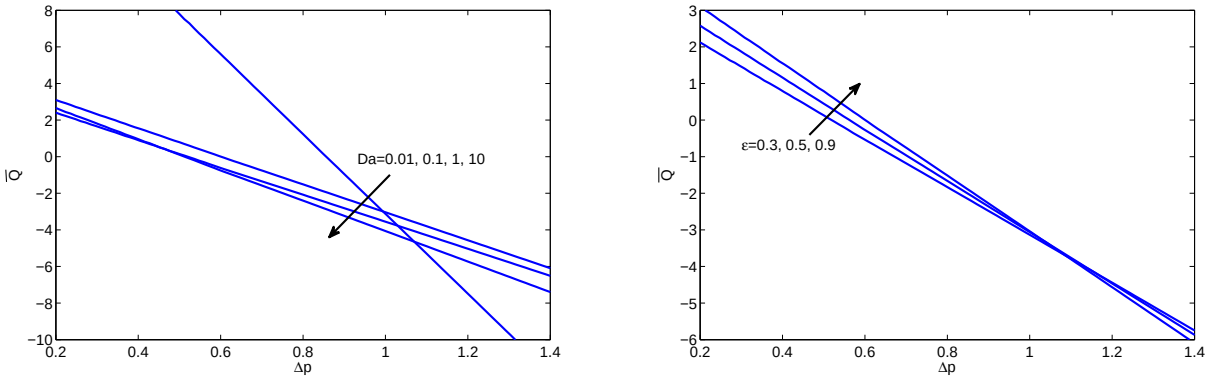

Figure 11: $\bar{Q}$ .vs. Δp with $\phi = 0.6, \gamma = 0.7, \tau_y = 0.001$ (a) for different Da ($\varepsilon = 0.7, \mu = 0.343, \beta = 0.5$) (b) for different ε ($\beta = 0.5, \mu = 0.343, Da = 0.1$).

4 Conclusion

In the present analysis we investigated the peristaltic flow of blood through microvessels. The radius of a microvessel is divided into two regions, the core region where blood behaves as a non-Newtonian Casson fluid model and a glycocalyx based peripheral layer where the blood behaves as a Newtonian fluid. We

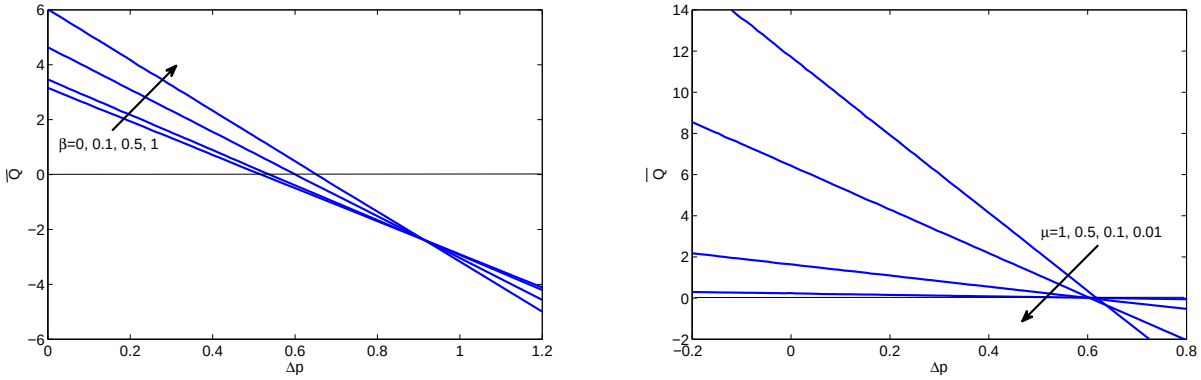

Figure 12: $\bar{Q}$ .vs. Δp with $\phi = 0.6, \gamma = 0.7, \tau_y = 0.001$ (a) for different β ($\varepsilon = 0.7, \mu = 0.343, Da = 0.1$) (b) for different μ ($\beta = 0.5, \varepsilon = 0.7, Da = 0.1$).

used both analytical and numerical techniques to solve the governing equations. We mainly discussed the effects of the Darcy number, stress-jump constant, porosity and the yield stress on the peristaltic flow. The trapping region decreases with increase of Darcy number but increases with the non-dimensional viscosity. Pumping efficiency increases with decrease of Darcy number while it is less for the clear fluid. These qualitative results may have significance to understand the transport of blood in small vessels.

5 Appendix

$$H = \left[(N_4+N_5)N_6 - N_2N_8\right]/N_{12},$$

$$G = (N_8 - N_7H)/N_6,$$

$$C = -1 + 2\tau_y h_1 + N_1\kappa\left(\cosh(\kappa h_1) - \cosh(\kappa h)\right) - G\alpha\left(\sinh(\alpha h) + \sinh(\alpha h_1)\right)$$

$$- H\alpha\left(\cosh(\alpha h) + \cosh(\alpha h_1)\right) + \frac{Ah_1{}^2}{2} - \frac{4\sqrt{\tau_y}}{3A}(Ah_1 + \tau_y)^{3/2},$$

$$N_1 = \frac{\varepsilon\mu_\varepsilon\kappa\psi_s E_z}{(\kappa^2-\alpha^2)\cosh(\kappa h)},$$

$$N_2 = \cosh(\alpha h) - \cosh(\alpha h_1) - \alpha\left(h\sinh(\alpha h) - h_1\sinh(\alpha h_1)\right),$$

$$N_3 = \sinh(\alpha h) - \sinh(\alpha h_1) - \alpha\left(h\cosh(\alpha h) - h_1\cosh(\alpha h_1)\right),$$

$$N_4 = q - h + \tau_y h_1{}^2 - N_1\left(\sinh(\kappa h) + \sinh(\kappa h_1)\right) + \kappa N_1\left(h\cosh(\kappa h) + h_1\cosh(\kappa h_1)\right),$$

$$N_5 = \frac{Ah_1{}^3}{3} - \frac{8\sqrt{\tau_y}}{15A^2}\left((Ah_1+\tau_y)^{5/2} - \tau_y{}^{5/2}\right) + \frac{4\sqrt{\tau_y}h_1}{3A}(Ah_1+\tau_y)^{3/2},$$

$N_6 = \mu_\varepsilon \alpha\,[\alpha\cosh(\alpha h_1) - \beta_1(\sinh(\alpha h_1) - \sinh(\alpha h))]$,

$N_7 = \mu_\varepsilon \alpha\,[\alpha\sinh(\alpha h_1) - \beta_1(\cosh(\alpha h_1) - \cosh(\alpha h))]$,

$N_8 = -(Ah_1 + 2\tau_y) - 2\sqrt{\tau_y}(Ah_1 + \tau_y)^{1/2} - N_1\kappa^2\mu_\varepsilon \sinh\kappa h_1 - \beta_1\mu_\varepsilon\,[1 + N_1\kappa(\cosh(\kappa h) - \cosh(\kappa h_1))]$,

$N_9 = \alpha^3\mu_\varepsilon \sinh(\alpha h)/N_6$, $N_{10} = -\alpha\cosh(\alpha h) - \alpha^3\mu_\varepsilon N_7 \sinh(\alpha h)/N_6$,

$N_{11} = N_9\,[N_1\kappa\mu_\varepsilon(\beta_1\cosh(\kappa h_1) - \kappa\sinh(\kappa h_1)) - \beta_1\mu_\varepsilon(1 + N_1\kappa\cosh(\kappa h))]$,

$N_{12} = N_3N_6 - N_2N_7$,

$N_{13} = N_{12} + N_{10}(N_6/N_{12})\,[q - h + N_1(h\kappa\cosh(\kappa h) - \sinh(\kappa h))]$,

$N_{14} = N_{10}(N_2/N_{14})\,[N_1\kappa\mu_\varepsilon(\kappa\sinh(\kappa h_1) + \beta_1\cosh(\kappa h) - \beta_1\cosh(\kappa h_1)) + \beta_1\mu_\varepsilon]$,

$N_{15} = -\tau_y h^2 + N_1(\sinh(\kappa h) + \sinh(\kappa h_1)) - \kappa N_1(h\cosh(\kappa h) + h_1\cosh(\kappa h_1))$,

$N_{16} = \alpha\,[N_7(\sinh(\alpha h) + \sinh(\alpha h_1)) - N_6(\cosh(\alpha h) + \cosh(\alpha h_1))]$,

$N_{17} = -1 + 2\tau_y h_1 + N_1\kappa(\cosh(\kappa h_1) - \cosh(\kappa h)) + \frac{Ah_1^2}{2} + \frac{4\sqrt{\tau_y}}{3A}(Ah_1 + \tau_y)^{3/2} - (4/3)\tau_y{}^2 A$,

$N_{18} = \alpha(\sinh(\alpha h) + \sinh(\alpha h_1))$,

$k_1 = 1 + h_1N_9 - h_1N_2(N_{10}/N_{12}) + ({h_1}^3/3)N_6(N_{10}/N_{12})$,

$k_2 = -N_{13} + (N_{10}/N_{12})\left[\tau_y {h_1}^2 - N_1(\sinh(\kappa h_1) - \kappa h_1\cosh(\kappa h_1))\right] + 2\tau_y(N_9 - N_2N_{10}/N_{12})$,

$k_3 = 2\sqrt{\tau_y}(N_9 - N_2N_{10}/N_{14})$, $k_4 = -\frac{8\sqrt{\tau_y}}{15}(N_6N_{10}/N_{14})$,

$k_5 = \frac{4h_1\sqrt{\tau_y}}{3}(N_6N_{10}/N_{14})$, $k_6 = \frac{8{\tau_y}^3}{15}(N_6N_{10}/N_{14})$,

$M_1 = \cosh\alpha - \cosh(\alpha\gamma) - \alpha(\sinh\alpha - \gamma\cosh(\alpha\gamma))$,

$M_2 = \sinh\alpha - \sinh(\alpha\gamma) - \alpha(\cosh\alpha - \gamma\cosh(\alpha\gamma))$,

$M_3 = \mu_\varepsilon\alpha\,[\alpha\cosh(\alpha\gamma) - \beta_1(\sinh(\alpha\gamma) - \sinh\alpha)]$,

$M_4 = \mu_\varepsilon\alpha\,[\alpha\sinh(\alpha\gamma) - \beta_1(\cosh(\alpha\gamma) - \cosh\alpha)]$,

$M_5 = -(A\gamma + 2\tau_y) - 2\sqrt{\tau_y}(A\gamma + \tau_y)^{1/2} - N_1\kappa^2\mu_\varepsilon\sinh(\kappa\gamma) - \beta_1\mu_\varepsilon\,[1 + N_1\kappa(\cosh\kappa - \cosh(\kappa\gamma))]$,

$M_6 = M_3\,[-\alpha(1-\gamma)(M_3\cosh\alpha - M_4\sinh\alpha) + M_3(\sinh\alpha - \sinh(\alpha\gamma))]$

$+M_3M_4(\cosh\alpha + \cosh(\alpha\gamma)) - M_3(M_2M_3 - M_1M_4)$,

$M_7 = -(M_2M_3 - M_1M_4)(M_3 + M_3N_1\kappa\cosh\kappa + M_5\alpha\sinh\alpha) - \alpha M_3(M_3\cosh\alpha - M_4\sinh\alpha)$,

$M_8 = 1 + N_1(\kappa\cosh\kappa - \sinh\kappa) - \tau_y\gamma^2 + N_1(1-\kappa\gamma)\sinh(\kappa\gamma) + \alpha M_1 M_5(M_3\cosh\alpha - M_5\sinh\alpha)$,

$M_9 = M_7 + M_8 - \frac{4}{3}A\gamma^2 + \frac{8\sqrt{\tau_y}}{15A^2}(A\gamma+\tau_y)^{5/2} - \frac{4\gamma\sqrt{\tau_y}}{3A}(A\gamma+\tau_y)^{3/2} - \frac{8{\tau_y}^3}{15A^2}$,

$M_{10} = N_1(\sinh\kappa - \sinh(\kappa\gamma)) + \cosh\alpha - \cosh(\alpha\gamma)$,

$M_{11} = M_3(\sinh\alpha - \sinh(\alpha\gamma)) + M_4(\cosh\alpha + \cosh(\alpha\gamma))$,

$M_{12} = 1 - \tau_y\gamma^2 + N_1\left[\kappa(\cosh\kappa - \gamma\cosh(\kappa\gamma)) - \sinh\kappa + \sinh(\kappa\gamma)\right]$,

$M_{13} = \frac{A\gamma^3}{3} + \frac{8\sqrt{\tau_y}}{15A^2}\left[(A\gamma+\tau_y)^{5/2} - {\tau_y}^{5/2}\right] - \frac{4\gamma\sqrt{\tau_y}}{3A}(A\gamma+\tau_y)^{3/2}$,

$M_{14} = M_3(\sinh\alpha - \sinh(\alpha\gamma)) + M_4(\cosh\alpha + \cosh(\alpha\gamma))$

References

1. Misra, JC, Pandey, SK, 2002, Peristaltic transport of blood in small vessels : study of a mathematicsl model, Comp. Math. with Appl., 43, 1183-1193.

2. Jaffrin, MY, Shapiro, AH, 1971, Peristaltic pumping, Ann. Rev. Fluid Mech., 3, 13-36.

3. Tripathi, D, Beg, O Anwar, 2013, Transient magneto-peristaltic flow of couple stress biofluids: A magneto-hydro-dynamical study on digestive transport phenomena, Mathematical Biosciences, 246, 72-83.

4. Misra, JC, Pandey, SK, 2001, Peristaltic flow of a multilayered power-law fluid through a cylindrical tube, Int. J Engng. Sci., 22, 387-402.

5. Batra, SK, 1974, Sperm transport through vas deferens. Review of hypotheses and suggestions for a quantitative model, Fertility Sterility, 25, 186-202.

6. Pozrikidis, C, 1987, A study of peristaltic flow, J. Fluid Mech., 180, 515-527.

7. Macht, DT, 1917, A contribution to the physiology of the ureter and vas deferens, J. Urol., 1, 97-111.

8. Chakravarty, S, Mandal,PK, Two-dimensional blood flow through tapered arteries under stenotic conditions, International Journal of Non-Linear Mechanics, 35 (2000) 779-793.

9. Mandal, PK, An unsteady analysis of non-Newtonian blood flow through tapered arteries with a stenosis, Int. J of Non-Linear Mech., 40 (2005) 151 - 164.

10. Shaw, S, Murthy, PVSN, Pradhan, SC, The effect of body acceleration on two dimensional flow of casson fluid through an artery with asymmetric stenosis, The Open Transport Phenomena Journal, The Open Conservation Biology Journal, 2 (2010) 55-68.

11. Deshikachar, KS, RamachandraRao, A., Effect of a magnetic field on the flow and blood oxygenation in channels of variable cross-section, International Journal of Engineering Science, 23 (1985) 1121-1133.

12. Mekheimer, KS, Peristaltic flow of blood under effect of a magnetic field in a non-uniform channels, Appl. Math and Comput., 153 (2004) 763-777.

13. Usha, S, Rao, AR, 1995, Peristaltic transport of a biofluid in a pipe of elliptic cross section, J. Biomech., 28 (1995) 45-52.

14. Akbar, NS, Razab, M., Ellahi, R, Influence of induced magnetic field and heat flux with the suspension of carbon nanotubes for the peristaltic flow in a permeable channel, Journal of Magnetism and Magnetic Materials, 381 (2015) 405-415.

15. Bhatti, M.M., Zeeshan, A., Ijazb, N, Slip effects and endoscopy analysis on blood flow of particle-fluid suspension induced by peristaltic wave, Journal of Molecular Liquids, 218 (2016) 240-245.

16. Bhatti, MM, Zeeshan, A., Ellahi, R., Shit, GC, Mathematical modeling of heat and mass transfer effects on MHD peristaltic propulsion of two-phase flow through a Darcy-Brinkman-Forchheimer porous medium, Advanced Powder Technology, 29 (2018) 1189-1197.

17. Mohammadein, SA, Abu-Nab, AK, Peristaltic Flow of a Newtonian Fluid Through a Porous Medium Surrounded Vapour Bubble in a Curved Channel, Journal of Nanofluids, 8 (2019) 651-656.

18. Casson, M, 1959, Rheology of Dispersive Systems, (Edited by C.C. Mills), p. 84, Pergamon, Oxford.

19. Fahraeus, R, 1929, The suspension stability of the blood. Physiol. Rev., 9, 241-274.

20. Fahraeus, R, Lindqvist, T, 1931, The viscosity of the blood in narrow capillary tubes,. Am. J Physiol., 96, 562-568.

21. Pries, AR, Secomb,TW, Gaehtgens, P, 1996, Biophysical aspects of blood flow in the microvasculature, Cardiovasc. Res., 32, 654-667.

22. Mishra, A, Rao, AR, 2005, Peristaltic transport in a channel with porous peripheral layer : model of a flow in gastrointestinal tract, J. Biomech., 38, 779-789.

23. Nield, DA, 2002, Modelling fluid flow in saturated porous media and at interfaces. D.B. Ingham, I. Pop (Eds.), Transport Phenomena in Porous Media II. Pergamon, Oxford, pp. 1-19.